Published in final edited form as:
Clin Cancer Res. 2009 January 15; 15(2): 476–484. doi:10.1158/1078-0432.CCR-08-0930.

Mitochondrial mutations contribute to HIF1α accumulation via increased reactive oxygen species and upregulated PDK2 in head and neck squamous cell carcinoma

Wenyue Sun[1], **Shaoyu Zhou**[1], **Steven S. Chang**[1], **Thomas McFate**[2], **Ajay Verma**[2], and **Joseph A. Califano**[1]

[1]Department of Otolaryngology–Head and Neck Surgery, Johns Hopkins Medical Institutions, Baltimore, MD 21287

[2]Department of Neurology, Uniformed Services University of the Health Sciences, Bethesda, MD 20814.

Abstract

Purpose—Mitochondrial mutations have been identified in head and neck squamous cell carcinoma (HNSCC), but the pathways by which phenotypic effects of these mutations are exerted remain unclear. Previously, we found that mitochondrial ND2 mutations in primary HNSCC increased reactive oxygen species (ROS) and conferred an aerobic, glycolytic phenotype with HIF1α accumulation and increased cell growth. The purpose of present study was to examine the pathways relating these alterations.

Experimental Design—Mitochondrial mutant and wild-type ND2 constructs were transfected into oral keratinocyte immortal cell line OKF6 and head and neck cancer cell line JHU-O19 and established transfectants. The protein levels of HIF1α, pyruvate dehydrogenease (PDH), phospho-PDH, and pyruvate dehydrogenease kinase (PDK) 2, together with ROS generation, were compared between the mutant and wild type. Meanwhile, the effects of small molecule inhibitors targeting PDK2, and mitochondrial targeted catalase, were evaluated on the ND2 mutant transfectants.

Results—We determined that ND2 mutant downregulated PDH expression via upregulated PDK2, with an increase in phospho-PDH. Inhibition of PDK2 with dichloroacetate decreased HIF1α accumulation and reduced cell growth. Extracellular treatment with hydrogen peroxide, a ROS mimic, increased PDK2 expression and HIF1α expression, and introduction of mitochondrial targeted catalase decreased mitochondrial mutation mediated PDK2 and HIF1α expression and suppressed cell growth.

Conclusions—Our findings suggest that mitochondrial ND2 mutation contributes to HIF1α accumulation via increased ROS production, upregulation of PDK2, attenuating PDH activity, thereby increasing pyruvate, resulting in HIF1α stabilization. This may provide insight into a potential mechanism by which mitochondrial mutations contribute to HNSCC development.

Requests for reprints: Joseph A. Califano, Department of Otolaryngology-Head and Neck Surgery, Johns Hopkins Medical Institutions, Baltimore, MD 21287. Phone: 410-955-6420; Fax: 410-955-8510; E-mail: jcalifa@jhmi.edu

Statement of Clinical Relevance Mitochondrial DNA (mtDNA) mutations occur with high frequency in a variety of human tumors but the functional consequences of such mutations are unknown. We reported here the novel mechanism of mitochondrial mutation-mediated cancer carcinogenesis. The mtDNA mutations contribute to malignant phenotype via increased ROS, upregulation of PDK2, attenuating PDH activity, elevating pyruvate production, and thereby HIF1α stabilization. Interestingly, ROS scavenger, PDK2 inhibitor dichloroacetate, and HIF1α small molecule inhibitor inhibit the malignant phenotypes induced by mitochondrial mutations. Our results not only provide mechanistic insight into the functional role of mtDNA mutations in human cancers but also open an important avenue for pharmacological perturbation of this important pathway, which benefits the patients harboring mtDNA mutations.

Keywords

Mitochondrial mutation; Head and neck cancer; HIF1α; Glycolysis; Pyruvate; Reactive oxygen species; PDK2

Introduction

Human mitochondrial DNA (mtDNA) is a circular double stranded DNA ~16.6 kb in size. It encodes 13 polypeptides, which includes seven subunits (ND1-ND6, ND4L) of respiratory chain complex I, one subunit (CYTB) of complex III, three subunits (COI-III) of complex IV and two subunits (ATP6 and 8) of complex V, 22 tRNAs and 2 rRNAs (1). Human mtDNA is more susceptible to damage than nuclear DNA as the mtDNA molecule is not protected by histones, is exposed to reactive oxygen species (ROS) generated during oxidative phosphorylation, and is replicated by DNA polymerase γ that copies with low fidelity due to the absence of a proof-reading function (2).

Somatic mtDNA mutations have been increasingly observed in primary human cancers (3). In head and neck squamous cell carcinoma (HNSCC), studies have shown a frequency of mitochondrial mutations ranging from 21-51%. Of note, our recent study found a nonrandom distribution of mitochondrial mutation throughout the mitochondrial enzyme complex components (4), and the majority of mitochondrial mutations occur during or after the transition of preneoplastic epithelium to cancer in HNSCC, indicating that these are a late event in HNSCC carcinogenesis (5).

Mitochondrial defects have long been suspected to play an important role in the development of cancer. Over 70 years ago, Otto Warburg described that cancer cells had impaired mitochondrial respiratory function compared with normal cells (6). He noted that cancer cells typically depend more on increased rates of glycolysis even in the presence of available oxygen, a phenomenon known as aerobic glycolysis or the Warburg effect. The Warburg effect is now considered a common property of cancer metabolism (7). Recently, studies from Lu et al. suggested that glycolytic products, like pyruvate, leads directly to HIF1α activation, which further boosts metabolism, and also stimulates angiogenesis and invasiveness, and in turn confers a growth advantage to cells (8).

Previously, we reported that nuclear transcribed, mitochondrial targeted mitochondrial ND2 protein mutants could induce increased ROS generation, elevated glycolytic metabolism, and enhanced HIF1α accumulation (4). The purpose of the present study was to discover the functional network mediated by mitochondrial mutation elucidating the above phenomenon. Here, we report that this mitochondrial mutation contributes to HIF1α accumulation via increased ROS production, upregulation of PDK2 (pyruvate dehydrogenase kinase 2), decreasing PDH (pyruvate dehydrogenase) activity, and elevating pyruvate concentration resulting in HIF1α stabilization.

Materials and methods

Cell culture

HeLa cells were grown in DMEM supplemented with 10% FBS. Human HNSCC cancer cell line JHU-O19, established at the Johns Hopkins University Department of Otolaryngology–Head and Neck Surgery, were grown in RPMI medium 1640 supplemented with 10% FBS. Human oral keratinocyte immortal cell line OKF6, purchased from the Rheinwald laboratory (Brigham and Women's Hospital, Boston), were grown in defined keratinocyte serum-free medium with defined growth supplement and final Ca^{2+} concentration of 0.4 mM. All of the

cells were supplemented with 1% (v/v) penicillin/streptomycin. The components of Krebs-Henseleit buffer were: 5.5 mM glucose, 1.3 mM $CaCl_2$, 1.3 mM $MgCl_2$, 124 mM NaCl, 3.5 mM KCl, 1.25 mM K_2HPO_4, 26.3 mM $NaHCO_3$, pH 7.5, following bubbling with 5% CO_2 in air. Where indicated, glucose was replaced by the indicated concentrations of agents.

Antibodies and reagents

Mouse monoclonal anti-HIF1α antibodies were purchased from BD Biosciences. Rabbit polyclonal anti-PDK2 antibodies were purchased from Abgent. Rabbit polyclonal anti-catalase antibodies were obtained from Calbiochem. Rabbit polyclonal anti-phospho-PDH antibodies were generated from Dr. Verma's lab. Mouse monoclonal anti-PDH E1α subunit antibody, and 2′, 7′-dichlorofluorescein diacetate (DCFH-DA) were from Invitrogen. Dichloroacetate (DCA) and catalase from human erythrocytes were purchased from Sigma. HIF1α small molecule inhibitor, NSC134754 was obtained from National Cancer Institute (Fedrerick, MD, USA) through their Developmental Therapeutic Program. Mitochondria-targeted catalase construct was gifted from Dr. Lenzen (Hannover Medical School, Hannover, Germany).

Plasmid construction

We converted the ND2 gene into nuclear code directly by using long-range gene synthesis as previously described (4). With this long-range gene synthesis technique, we synthesized ND2 wild type and one mutant, mt1 (ND2-G4776A; amino acid change A-T). The synthesized wild type and mutants then were subcloned into SalI and NotI sites of plasmid pCMV/myc/mito (Invitrogen). Plasmids were resequenced with conventional sequencing to confirm results.

Transfection of ND2 constructs

HeLa cells, O19 cells, and OKF6 immortal keratinocyte were transfected with empty vector, wild-type, or mutant construct at 40–60% confluence by using FuGENE 6 (Roche) according to product protocols.

Pyruvate measurement

To measure pyruvate, 50 μl of medium was taken from cells grown in 2 ml of medium in six-well cell culture plates and frozen until the time of measurement. Before measurement, samples were centrifuged to remove any microbubbles. Pyruvate content was measured by the enzymatic method using a pyruvate kit (CMA microdialysis). Metabolite measurements were performed with the CMA 600 Analyzer.

ROS measurement

Intracellular ROS generation was assessed using DCFH-DA with the method described previously (9) . Briefly, cells were plated on Petri dishes and incubated with DCFH-DA (10 μM) under various conditions. The cells were lysed and centrifuged to remove debris, and the fluorescence in the supernatant was measured using a spectrofluorometer (excitation, 500 nm; emission, 530 nm). Data were normalized to values obtained from untreated controls.

Western blotting

Cells were lysed in RIPA buffer supplemented with proteinase inhibitor. ~30 μg of whole protein extract were resolved on a 4-10% NuPAGE gel (Invitrogen), transferred to a Polyvinylidene fluoride membrane (Amersham Biosciences), probed overnight at 4°C with the antibody against PDK2, PDH, p-PDH, HIF1α, catalase, actin, and then revealed using the enhanced chemiluminescence system (Roche). Densitometry was performed using using Image J software (NIH).

Sulforhodamine-B assay

Growth inhibition was evaluated using the sulforhodamine B assay as previously described (10). Briefly, cells were plated into clear flat-bottomed 96-well plates and left to attach overnight. They were treated with the indicated agents and incubated for 48-72 hours. At the end of the incubation period, the cells were fixed and stained with sulforhodamine B (Sigma). The absorbance value was read at a wavelength of 540 to 570 nm. The cell survival was presented as the percentage of control as calculated by using the equation: A_t/A_c x 100, where A_t and A_c represent the absorbance in treated and control cultures, respectively.

Tumor xenografts

For tumor growth, 2×10^6 cells in 100 μL PBS were injected s.c. at the left flank of 4- to 6-week-old female athymic nude mice (CD-1-nuBR, Charles River). All experiments were performed in accordance with the Johns Hopkins University Animal Care and Use Committee guideline. Each group consisted of 5 mice. Tumor growth was monitored weekly and mice showing signs of morbidity were immediately sacrificed according to University guidelines. Tumor volume was calculated with slide calipers using the following formula: V = Width x Width x Length x 0.5, where V is volume (mm^3).

Statistical analysis

Differences between experimental variables were estimated using Student's t test. A probability level of 0.05 was chosen for statistical significance. The columns in the histograms represent the mean ± SD of at least triplicate values from independent experiments.

Results

Mitochondrial ND2 mutant promotes head and neck cancer cell growth through HIF1α accumulation

Recently, we reported that expression of nuclear transcribed, mitochondrial targeted ND2 mutant resulted in anchorage independent growth and HIF1α accumulation. To further examine this phenomenon, one mitochondrial ND2 mutant construct (mt1: ND2-G4776A, amino acid change A→T, which were originally found in human primary HNSCC cancers), was established. We transfected this mutant into Hela cells, immortal keratinocyte OKF6 cells, and O19 head and neck cell line (ND2 wild type background) respectively. Western blot analysis showed that HIF1α was overexpressed in all three cells transfected mitochondrial ND2 mutant versus their corresponding wild-type ND2 construct (Figure 1A), with 3.0 ± 0.9-fold (Mean ± SD, n = 3, P = 0.012), 4.0 ± 1.7-fold (Mean ± SD, n = 3, P = 0.034), and 2.5 ± 0.4-fold (Mean ± SD, n = 3, P = 0.010) respectively. In consistent, the ND2 mutant exhibited increased proliferation rates as compared with the wild-type in Hela cells and O19 cells (Figure 1B and 1C, P < 0.01). In our study, we also found that Hela cells stably transfected with ND2 mutant significantly increased the tumor growth in nude mice compared with the wildtype (Supplementary Figure S1, P < 0.01). Further, we found that treatment with 0.5 μM HIF1α small molecule inhibitor, NSC134754, the cell growth advantage conferred by the mitochondrial ND2 mutant in Hela cells and O19 cells, was completely eliminated at 48 h (Figure 1B and 1C) (11). Taken together, these suggest that HIF1α accumulation is a major mechanism of mitochondrial mutation induced growth for ND2 mutants.

Of note, in our study (data not shown), we also sequenced the mitochondrial genome in 4 other HNSCC cell lines (JHU-O11, JHU-O12, UM-22A, UM-22B), and no cell line has been found to demonstrate the specific ND2 mutation we analyzed. The other cell line we have tested displays a variety of mitochondrial mutations in multiple respiratory complex enzymes, including ND2, with HIF1α expression. Due to the complex nature of multiple respiratory

enzyme mutations in this cell line and the confounding effect this may have on assessment of an introduced, overexpressed ND2 mutation, it is difficult to determine how this would be interpreted as specifically supporting our mechanism.

Mitochondrial ND2 mutant decreases PDH, increases phospho-PDH, and thereby increases pyruvate production, resulting in increased HIF1α accumulation

Recently, the cancer-specific aerobic glycolytic metabolism reported by Warburg has been linked to impairment of HIF1α degradation induced by 2-oxoglutarate analogs, such as pyruvate (12). We reasoned that the mitochondrial ND2 mutations may result in impaired respiration, resulting in accumulation of reduced NADH and pyruvate and HIF1α stabilization. Here, the pyruvate production was determined in OKF6 cells and O19 cells after transfection with ND2 mutant. We found significantly increased pyruvate production in ND2 mutant-transfected OKF6 cells (5.0 ± 0.4 versus 2.8 ± 0.2 μmol/mg protein, $P < 0.01$) and O19 cells (1.6 ± 0.1 versus 1.1 ± 0.1 μmol/mg protein, $P < 0.01$) compared with corresponding wild types (Figure 2A and 2B). To investigate whether increased pyruvate production could stimulate HIF1α accumulation, we administered exogenous pyruvate to OKF6 cells. HIF1α accumulation was induced by 2.9 ± 0.6-fold and 5.0 ± 1.1-fold after 4 h treatment with 0.25 mM or 0.5 mM pyruvate in glucose-free Krebs buffer (Figure 2C, $P < 0.05$). Previous studies have evidenced that PDH catalyses the irreversible oxidative decarboxylation of pyruvate to acetyl-CoA, thereby linking glycolysis to the tricarboxylic acid (TCA) cycle (13). It is generally believed that the pyruvate dehydrogenase reaction is the rate-limiting step in the aerobic stage of oxidation of carbohydrate fuels. To ask whether dysregulation of PDH contributed to the increased production of pyruvate, we evaluated the expression of PDH via western blot. Compared with wild-type ND2, ND2 mutant resulted in by 1.3 ± 0.2-fold, 1.4 ± 0.2-fold, and 1.3 ± 0.1-fold downregulation of PDH in Hela cells, OKF6 cells, and O19 cells respectively (Figure 2D, n= 3, $P < 0.05$). Because PDH has three phosphorylation sites including Ser264 (the most rapidly modified site), and can be inactivated by phosphorylation (13), we further tested whether ND2 mutation resulted in conversion of PDH to phospho-PDH, which in turn elevated pyruvate production. To this end, anti-phosphoser^{264}-PDH antibody was used to detect the expression levels of phospho-PDH in OKF6, Hela, and O19 cells after transient transfection with ND2 mutant. In comparison with the wild type, phospho-PDH was found 1.3 ± 0.1-fold, 1.7 ± 0.2-fold and 1.9 ± 0.2-fold higher overexpression in the cells with ND2 mutants (Figure 2D, n = 3, $P < 0.05$).

Mitochondria ND2 mutant elevated PDK2 expression contributing to HIF1α accumulation

PDK2, a PDH kinase, is the key enzyme responsible for phosphorylation of PDH at site Ser264 (14). Thus, we examined whether our mitochondrial ND2 mutant increased the expression of phospho-PDH through upregulation of PDK2. As shown in Figure 3A, elevated expression of PDK2 (1.8 ± 0.4-fold in Hela cells, n = 3, $P < 0.05$; 2.2 ± 0.2-fold in OKF6 cells, n = 3, $P < 0.01$; 2.3 ± 0.4-fold in O19 cells, n = 3, $P < 0.05$) was observed in all three cell lines transfected with the mitochondrial ND2 mutant, compared with the wild-type. This suggests that mitochondrial mutants may upregulate PDK2 expression, followed by attenuation of PDH activity and resulting in elevated pyruvate concentration, which in turn contributes to HIF1α stabilization. To determine whether PDK2 is essential for mitochondrial ND2 mutation-mediated HIF1α stabilization, we tested the effects of dichloroacetate, a PDK2 small molecule inhibitor (15). We found that, after treatment of O19 cells and OKF6 cells transfected with ND2 mutant with 2 mM dichloroacetate, the HIF1α expression level was significantly decreased (Figure 3B and Supplementary Figure S2A). Consistent with this result was our observation that the cell growth was inhibited in O19 cells transfected with ND2 mutant after 3 days' treatment with 4 mM dichloroacetate to a greater extent than was noted in wild type (Figure 3C). Likewise, we also observed the growth inhibition in OKF6 cells transfected with ND2 mutant after 2 days' treatment with 8 mM dichloroacetate (Supplementary Figure S2B).

Mitochondrial ND2 mutant upregulated PDK2 expression via increased ROS generation

We hypothesized that mitochondrial mutants may upregulate PDK2 through increased ROS generation. To test this possibility, we determined the ROS generation in OKF6 cells transiently transfected with mitochondrial mutant. As showed in Figure 4A, mitochondrial ND2 mutant resulted in ~20% percent higher ROS yield than that in the wild type ($P < 0.01$). To investigate the effect induced by the elevated ROS yield, H_2O_2 titration was performed to mimic the activity of mitochondrial ND2 mutation. We found that a dosage of 20-50 μM of H_2O_2, following a bolus administration, could reproduce similar ROS increase in OKF6 cells (Figure 4B). We then evaluated the PDK2 expression level in OKF6 cells, O19 cells and Hela cells treated with hydrogen peroxide at the concentrations of 0, 10, 20, 50 100 μM. Our results showed that after exposure to 20 and 50 μM H_2O_2, PDK2 was significantly increased in OKF6 cells, O19 cells, and Hela cells; consistently, HIF1α was also found to be upregulated after H_2O_2 exposure (Figure 4C, and Supplementary Figure S3).

Inhibition of ROS production in mitochondrial ND2 mutant attenuated PDK2 expression and HIF1α expression

To investigate the effect of reduction of ROS on cells expressing mitochondrial ND2 mutant, extracellular catalase treatment was utilized. Shown in Figure 5A, catalase treatment resulted in PDK2 downregulation significantly in O19 cells transfected with the mitochondrial ND2 mutant compared the wild-type. Because the mitochondrion is the main organelle of ROS generation, mitochondria-targeted catalase (mito-cat) construct was then employed for scavenging ROS produced in O19 cells transfected with mitochondrial mutant (Figure 5B) (16). Our western blot showed that, by introduction of mitocat, PDK2 expression was decreased by 1.8 ± 0.2-fold in ND2 mutant cells compared to the wild type ($n = 3$, $P < 0.05$). Moreover, we found that introduction of mito-cat in OKF6 cells expressing mitochondrial mutant, resulted in PDK2 downregulation, as well as decreased expression of HIF1α (Figure 5C). Further, we observed that introduction of mito-cat in O19 cells resulted in growth inhibition ($P<0.05$) that reversed mitochondrial mutant-mediated growth stimulation (Figure 5D). Taken together, these suggest that mitochondrial generated ROS plays a significant role in mitochondrial ND2 mutant-mediated head and neck cancer growth.

Discussion

Mitochondrial mutations have been identified extensively in human HNSCC cancers, yet the functional role of mitochondrial mutation in HNSCC cancer carcinogenesis remains unclear. HIF1α is overexpressed in most of the common human cancer types, including HNSCC (17). Multiple studies of HIF1α and head and neck cancer have shown a significant association between HIF1α overexpression and poor prognosis coupled to increased patient mortality, as well as resistance to treatment (18) (19). HIF1α participates in transcriptional activation of genes that are involved in crucial aspects of cancer biology, including angiogenesis, cell survival, glucose metabolism and invasion. In this study, we investigate the effect of mitochondrial mutation on HIF1α activation. Our data showed that HIF1α expression is enhanced in cells transfected with mutant mitochondrial ND2. Meanwhile, the ND2 mutant exhibited increased proliferation as comparison with the wild-type, although the wild-type ND2 increased relatively the cell growth in comparison to the vector alone, in which the reason is unknown. Use of a HIF1α small molecule blocked mitochondrial ND2 mutant mediated cancer cell growth (Figure 1). These suggest that mitochondrial ND2 mutation may induce head and neck cancer development through constitutive activation of HIF1α.

Lu et al. recently reported that one product generated by Warburg effect, pyruvate, could dramatically increased HIF1α accumulation in cancer cells by inhibiting the prolyl hydroxylase enzyme activity, which could result in degradation of HIF1α protein through hydroxylation

(12). Here we proposed that mitochondrial ND2 mutations via production of ROS, regulate enzymes including PDH and PDH kinase, which resulted in elevated pyruvate production contributing to HIF1α accumulation. First, either O19 head and neck cancer cells or OKF6 immortal cells, which were transfected with mitochondrial ND2 mutant, generated more pyruvate compared with the wild-type. Second, extracellular treatment of pyruvate led to upregulation of HIF1α. Third, PDH, which mediates the entry of pyruvate into TCA cycle, was downregulated in cells with mitochondrial ND2 mutant. Moreover, we found that phospho-PDH (inactive form of PDH) and PDK2 (PDH kinase; inactivate PDH through phosphorylation) were both upregulated in cells expressing the mitochondrial mutant.

Mitochondrial ND2 encodes the nicotinamide adenine dinucleotide dehydrogenase (NADH) subunit 2 protein, a hydrophobic subunit of respiratory chain complex I, proposed to reside near the junction between the membrane and the peripheral arm (that projects into the mitochondrial matrix) of the complex I (20). It is known that the mitochondrial respiratory chain is exquisitely tuned to transfer electrons from NADH or FADH to a series of electron acceptors, until the final transfer to oxygen leads to production of water, and also is known that these biochemical reactions can result in electron leakage and lead to the production of ROS (21) (22) (23). The ND2 subunit is suggested to be involved in proton pumping across the inner mitochondrial membrane because of its sequence homology with a class of Na^+/H^+ antiporters (20). Recently, Gusdon et al. showed that mouse ortholog of the protective allele (mt-ND2) played a critical role in the control of mitochondrial ROS production (24). In our study, we found that more ROS was generated in cells transfected with mitochondrial ND2 mutant compared with wild type. Extracellular treatment of cells with H_2O_2, a ROS mimic, led to increased HIF1α accumulation. Further, we found that expression of mitochondrial targeted catalase could inhibit HIF1α accumulation and impede cell growth, although a partial reversal of growth stimulation with excellular mito-catalase treatment was observed, likely due to the incomplete transfection efficiency during transient transfection experiments. These data suggested that mitochondrial mutation induces HIF1α accumulation through increased ROS production, consistent with results reported by Brunelle et al. that the expression of catalase prevented the hypoxic stabilization of HIF1α (25). In this study, enhanced ROS induced respiratory malfunction, resulting in blockage of the TCA cycle, ultimately led to pyruvate accumulation and HIF1α stabilization.

To ask whether there are other pathways mediated by ROS inducing increased pyruvate production and HIF1α accumulation, we also investigated the effect of ROS on PDK2 expression. We found that extracellular treatment of H_2O_2 led to increased PDK2 expression. Meanwhile, application of dichloroacetate, a PDK2 small molecule inhibitor which previously was reported to induce apoptosis and decrease proliferation (26) to cells transfected with mitochondrial ND2 mutant, resulted in decreased HIF1α accumulation and inhibition of cell growth. These suggested that increased ROS production may contribute to HIF1α stabilization through upregulation of PDK2. It is likely that the upregulation of PDK2 attenuated PDH activity and triggered increased pyruvate production, which in turn lead to HIF1α stabilization. As a minor point, we also observed that with the PDK2 inhibitor dichloroacetate, there was still relatively increased proliferation in O19 mutant transfectant cells compared with the O19 wildtype transfectants (Figure 3C). This may suggest that that there existed other pathways participating mitochondrial mutation-mediated cell proliferation.

In summary, our study suggested the mechanism of the mitochondrial mutation-mediated HNSCC carcinogenesis through HIF1α stabilization: (1) enhanced ROS leads to pyruvate accumulation through blocking TCA cycle, hence resulting in HIF1α stabilization; (2) increased ROS production upregulates PDKs, followed by attenuating PDH activity and triggering high pyruvate concentration, which in turn contribute to HIF1α stabilization (Figure 6). However, we do not rule out the increase in ROS stimulates constitutive activation of

HIF1α through other pathways. Further study on this may help us better understand the functional role of mitochondrial mutation in the development of an invasive phenotype.

Supplementary Material

Refer to Web version on PubMed Central for supplementary material.

Acknowledgments

We thank Dr. Sigurd Lenzen for generously supplying the mitochondrial targeted catalase construct and Dr. Marianna Zahurak for kind assistance with statistical analysis.

Grant support: Specialized Program of Research Excellence grant P50 CA96784. J.A. Califano is a Damon Runyon-Lilly Clinical Investigator supported by the Damon Runyon Cancer Research Foundation (CI-#9), a Clinical Innovator Award from the Flight Attendant Medical Research Institute, and National Institute of Dental and Craniofacial Research grant 1R01DE015939-01.

References

1. Wallace DC. Mitochondrial diseases in man and mouse. Science 1999;283:1482–8. [PubMed: 10066162]
2. Jiang WW, Califano J. Mitochondrial mutations and nasopharyngeal carcinoma. Cancer Biol Ther 2004;3:1275–6. [PubMed: 15662125]
3. Chatterjee A, Mambo E, Sidransky D. Mitochondrial DNA mutations in human cancer. Oncogene 2006;25:4663–74. [PubMed: 16892080]
4. Zhou S, Kachhap S, Sun W, et al. Frequency and phenotypic implications of mitochondrial DNA mutations in human squamous cell cancers of the head and neck. Proc Natl Acad Sci U S A 2007;104:7540–5. [PubMed: 17456604]
5. Mithani SK, Taube JM, Zhou S, et al. Mitochondrial mutations are a late event in the progression of head and neck squamous cell cancer. Clin Cancer Res 2007;13:4331–5. [PubMed: 17671113]
6. Warburg O. On respiratory impairment in cancer cells. Science 1956;124:269–70. [PubMed: 13351639]
7. Pan JG, Mak TW. Metabolic targeting as an anticancer strategy: dawn of a new era? Sci STKE 2007;2007:pe14. [PubMed: 17426345]
8. Lu H, Forbes RA, Verma A. Hypoxia-inducible factor 1 activation by aerobic glycolysis implicates the Warburg effect in carcinogenesis. J Biol Chem 2002;277:23111–5. [PubMed: 11943784]
9. Chandel NS, McClintock DS, Feliciano CE, et al. Reactive oxygen species generated at mitochondrial complex III stabilize hypoxia-inducible factor-1alpha during hypoxia: a mechanism of O2 sensing. J Biol Chem 2000;275:25130–8. [PubMed: 10833514]
10. Whitehurst AW, Bodemann BO, Cardenas J, et al. Synthetic lethal screen identification of chemosensitizer loci in cancer cells. Nature 2007;446:815–9. [PubMed: 17429401]
11. Chau NM, Rogers P, Aherne W, et al. Identification of novel small molecule inhibitors of hypoxia-inducible factor-1 that differentially block hypoxia-inducible factor-1 activity and hypoxia-inducible factor-1alpha induction in response to hypoxic stress and growth factors. Cancer Res 2005;65:4918–28. [PubMed: 15930314]
12. Lu H, Dalgard CL, Mohyeldin A, McFate T, Tait AS, Verma A. Reversible inactivation of HIF-1 prolyl hydroxylases allows cell metabolism to control basal HIF-1. J Biol Chem 2005;280:41928–39. [PubMed: 16223732]
13. Patel MS, Korotchkina LG. Regulation of the pyruvate dehydrogenase complex. Biochem Soc Trans 2006;34:217–22. [PubMed: 16545080]
14. Korotchkina LG, Patel MS. Site specificity of four pyruvate dehydrogenase kinase isoenzymes toward the three phosphorylation sites of human pyruvate dehydrogenase. J Biol Chem 2001;276:37223–9. [PubMed: 11486000]
15. Baker JC, Yan X, Peng T, Kasten S, Roche TE. Marked differences between two isoforms of human pyruvate dehydrogenase kinase. J Biol Chem 2000;275:15773–81. [PubMed: 10748134]

16. Guzy RD, Hoyos B, Robin E, et al. Mitochondrial complex III is required for hypoxia-induced ROS production and cellular oxygen sensing. Cell Metab 2005;1:401–8. [PubMed: 16054089]
17. Zhong H, De Marzo AM, Laughner E, et al. Overexpression of hypoxia-inducible factor 1alpha in common human cancers and their metastases. Cancer Res 1999;59:5830–5. [PubMed: 10582706]
18. Hui EP, Chan AT, Pezzella F, et al. Coexpression of hypoxia-inducible factors 1alpha and 2alpha, carbonic anhydrase IX, and vascular endothelial growth factor in nasopharyngeal carcinoma and relationship to survival. Clin Cancer Res 2002;8:2595–604. [PubMed: 12171890]
19. Aebersold DM, Burri P, Beer KT, et al. Expression of hypoxia-inducible factor-1alpha: a novel predictive and prognostic parameter in the radiotherapy of oropharyngeal cancer. Cancer Res 2001;61:2911–6. [PubMed: 11306467]
20. Brandt U. Energy converting NADH:quinone oxidoreductase (complex I). Annu Rev Biochem 2006;75:69–92. [PubMed: 16756485]
21. Flemming D, Stolpe S, Schneider D, Hellwig P, Friedrich T. A possible role for iron-sulfur cluster N2 in proton translocation by the NADH: ubiquinone oxidoreductase (complex I). J Mol Microbiol Biotechnol 2005;10:208–22. [PubMed: 16645316]
22. Mathiesen C, Hagerhall C. Transmembrane topology of the NuoL, M and N subunits of NADH:quinone oxidoreductase and their homologues among membrane-bound hydrogenases and bona fide antiporters. Biochim Biophys Acta 2002;1556:121–32. [PubMed: 12460669]
23. Friedrich T. Complex I: and chimaera of a redox and conformation-driven proton pump? J Bioenerg Biomembr 2001;33:169–77. [PubMed: 11695826]
24. Gusdon AM, Votyakova TV, Reynolds IJ, Mathews CE. Nuclear and mitochondrial interaction involving mt-Nd2 leads to increased mitochondrial reactive oxygen species production. J Biol Chem 2007;282:5171–9. [PubMed: 17189252]
25. Brunelle JK, Bell EL, Quesada NM, et al. Oxygen sensing requires mitochondrial ROS but not oxidative phosphorylation. Cell Metab 2005;1:409–14. [PubMed: 16054090]
26. Bonnet S, Archer SL, Allalunis-Turner J, et al. A mitochondria-K+ channel axis is suppressed in cancer and its normalization promotes apoptosis and inhibits cancer growth. Cancer Cell 2007;11:37–51. [PubMed: 17222789]

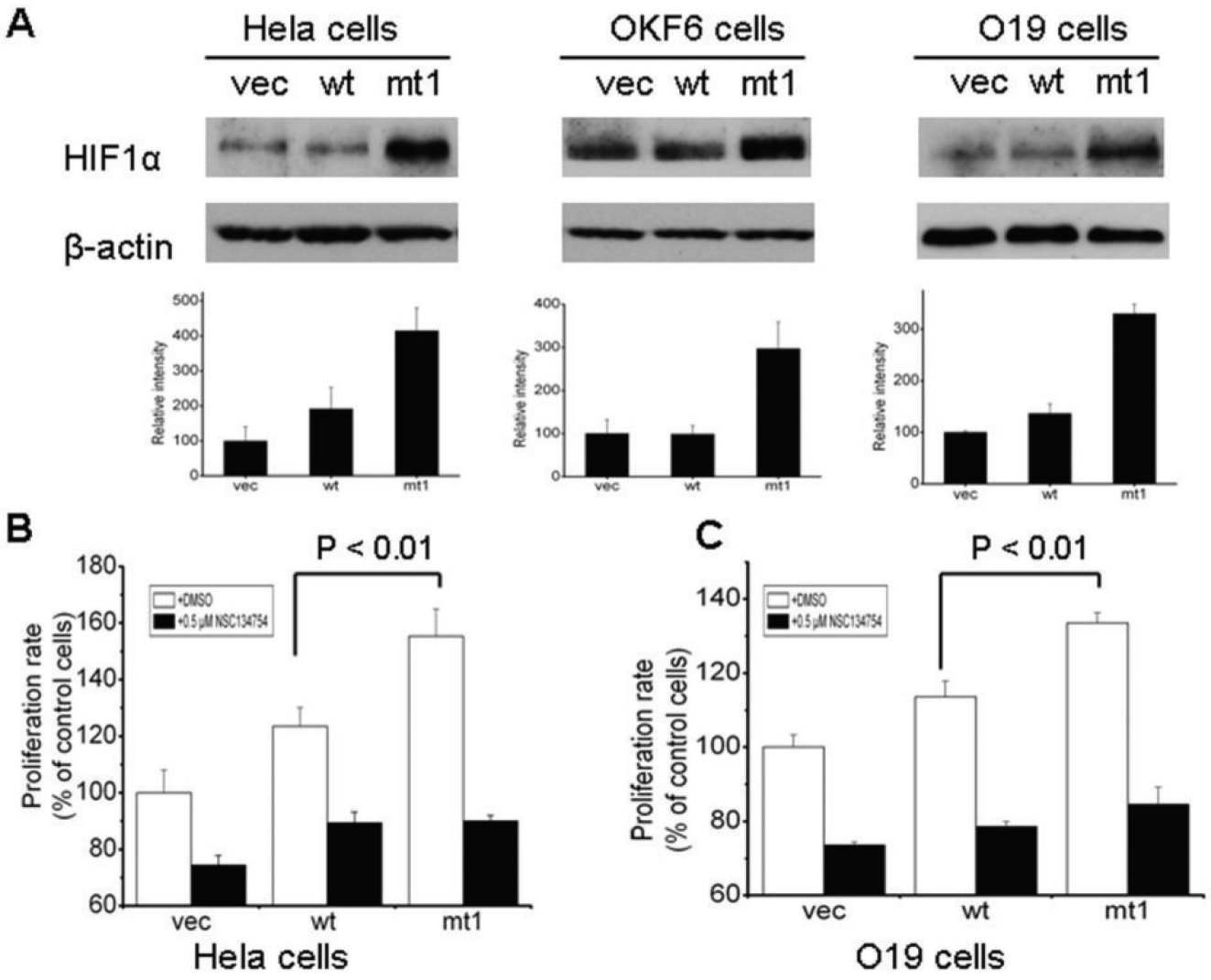

Figure 1.

Mitochondrial ND2 mutant promoted head and neck cancer cell growth through HIF1α accumulation. A, the protein levels of HIF1α were determined 4 h following switching from culture medium to Krebs-Henseleit buffer in Hela, OKF6, and O19 cells. Immunoblots were quantified via densitometry and ImageJ software. HIF1α was overexpressed by 3.0 ± 0.9-fold, 4.0 ± 1.7-fold, and 2.5 ± 0.4-fold in the three cells transfected mitochondrial ND2 mutant versus their corresponding wild type ($n = 3$, $P < 0.05$). Representative images from three independent experiments were shown. B, the growth of Hela cells stably transfected with ND2 mutant, was inhibited after treatment with NSC134754, a HIF1α small inhibitor. Cell growth was estimated by using a sulforhodamine B assay, after exposure for 48 h to 0.5 μM of NSC134754. C, the growth of O19 cells with ND2 mutant, was inhibited after treatment with NSC134754. Cell growth was estimated by staining with sulforhodamine B, after exposure for 48 h to 0.5 μM of NSC134754. Data are mean ± SD values from three independent experiments. Student's t test showed significance between mutant and wild type ($P < 0.01$) in the absence of NSC134754 whereas no significance in the presence of NSC134754. Vec, vector alone; wt, wild-type; mt1, mutant.

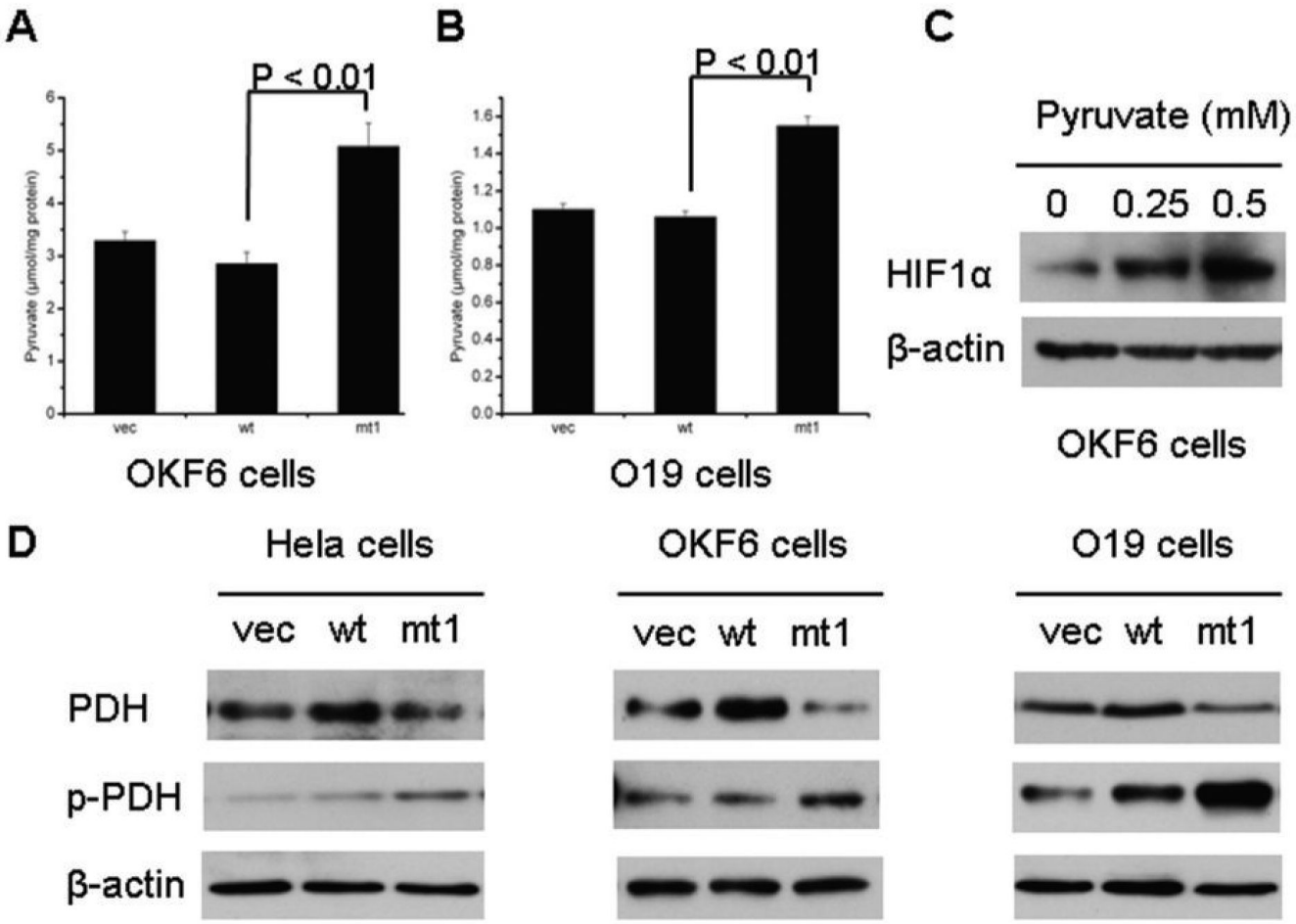

Figure 2.

Mitochondrial ND2 mutant decreased PDH, increased phospho-PDH, and thereby increased pyruvate production, resulting in increased HIF1α accumulation. A and B, the production of pyruvate in the culture buffer was measured in OKF6 cells and O19 cells. Twenty-four hours after transiently transfection with ND2 mutant and wild type construct, the cells were allowed to grow in pyruvate-free media for 24 h, and then media were collected and assayed for concentration of pyruvate. Data represent mean ± SD of three individual experiments. Student's t test showed significance between mutants and wild type ($P < 0.01$). C, OKF6 cells were cultured for 4 h in glucose-free Krebs buffer containing 0.25 or 0.5 mM pyruvate. HIF-1α levels were determined after 4 h of culture. Treatment with 0.25 and 0.5 mM pyruvate caused HIF-1α accumulation by 2.9 ± 0.6-fold and 5.0 ± 1.1-fold respectively, as revealed by densitometry and ImageJ software analysis. D, western blot for PDH and phospho-PDH. Mutant 1 (mt1) transfection of HeLa, OKF6 and O19 cells induced decrease of PDH and increase of phosphor-PDH, compared with wild type (wt). After 48 h of transfection, cells were incubated with glucose-free Krebs buffer for 4 h. The cells then were harvested for western blotting as described in Materials and Methods. Results are representative of three independent experiments.

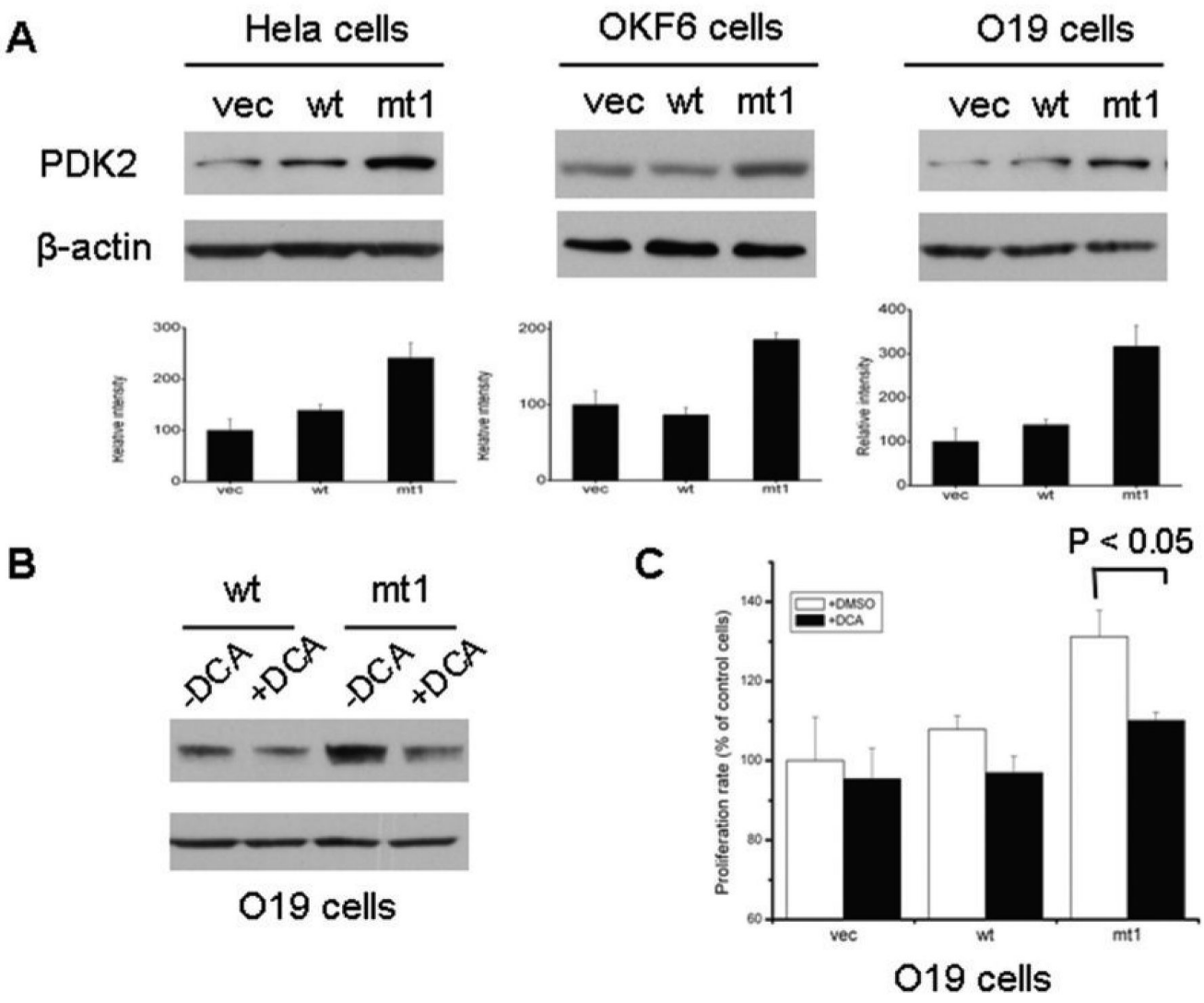

Figure 3.

Mitochondria ND2 mutant elevated PDK2 expression contributing to HIF1α accumulation. A, the protein levels of PDK2 were determined 4 h following switching from culture medium to Krebs-Henseleit buffer in O19, Hela, and OKF6 cells. Data were reported as mean ± SD of three replicate experiments. B, HIF1α levels in O19 cells stably transfected with ND2 mutant and wild type constructs, exposed to 2 mM dichloroacetate (DCA) for 24 h. C, the growth of O19 cells, which were stably transfected with ND2 mutant, was significantly ($P<0.05$) inhibited after treatment with 4 mM dicloroacetate for 72 h. Data represent mean ± SD of three individual experiments.

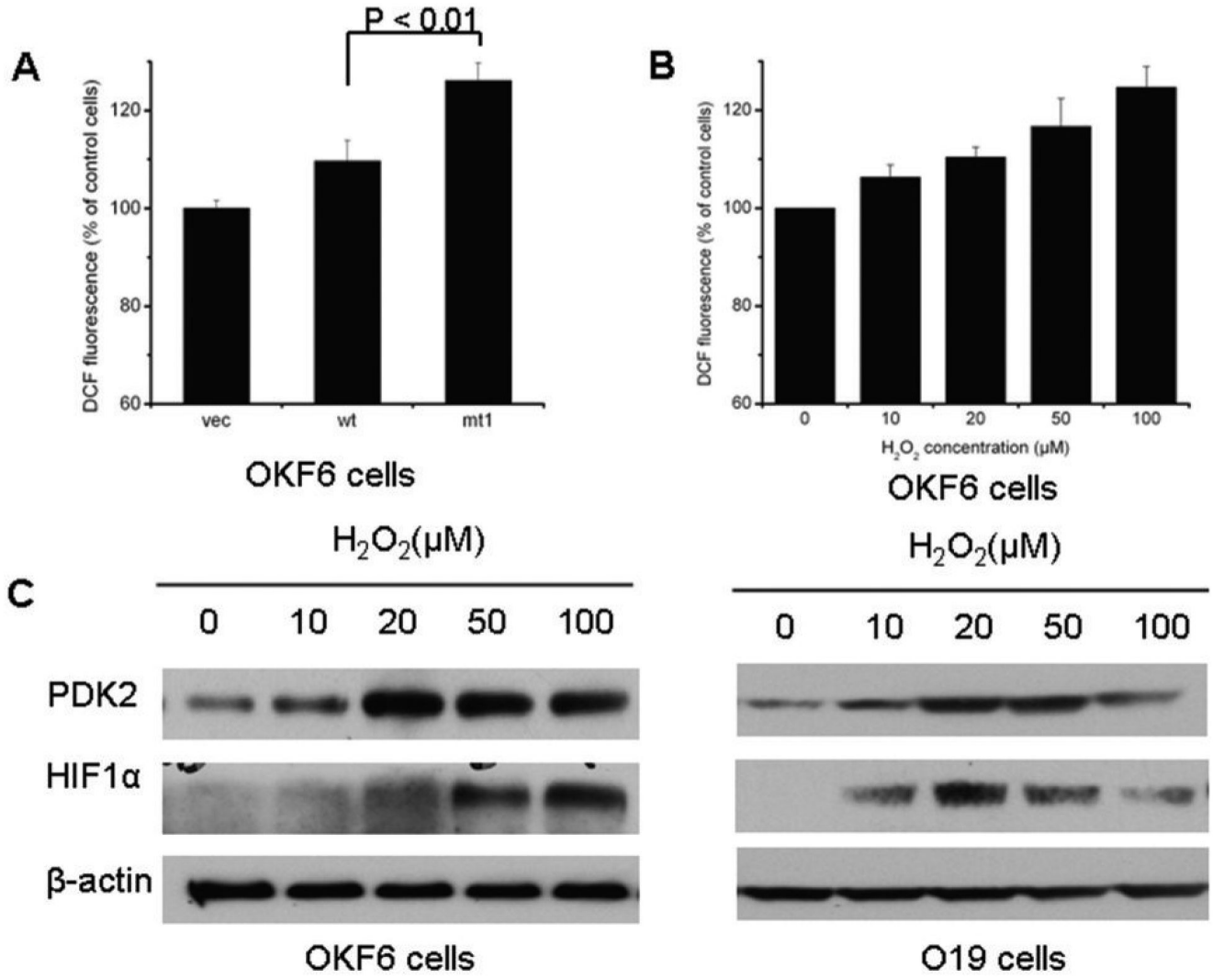

Figure 4.

Mitochondrial ND2 mutant upregulated PDK2 expression via increased ROS generation. A, ROS generation in ND2-transfected OKF6 cells measured by fluorescent spectrometer. Forty-eight hours posttransfection, cells were harvested, and ROS was measured with a fluorescence probe DCFH-DA. Data represent mean ± SD of three individual experiments. Student's t test showed significance between mutant and wild type ($P < 0.01$). B, ROS production in OKF6 cells exposed to repeated boluses of H_2O_2 (0, 10, 20, 50, 100 μM) every 20 min for 2 h. C, PDK2 and HIF1α levels in OKF6 cells (left panel) and O19 cells (right panel) following a bolus administration of H_2O_2 (0, 10, 20, 50, 100 μM) for 2 h. Blots were probed for HIF1α, PDK2, and β-actin as a loading control.

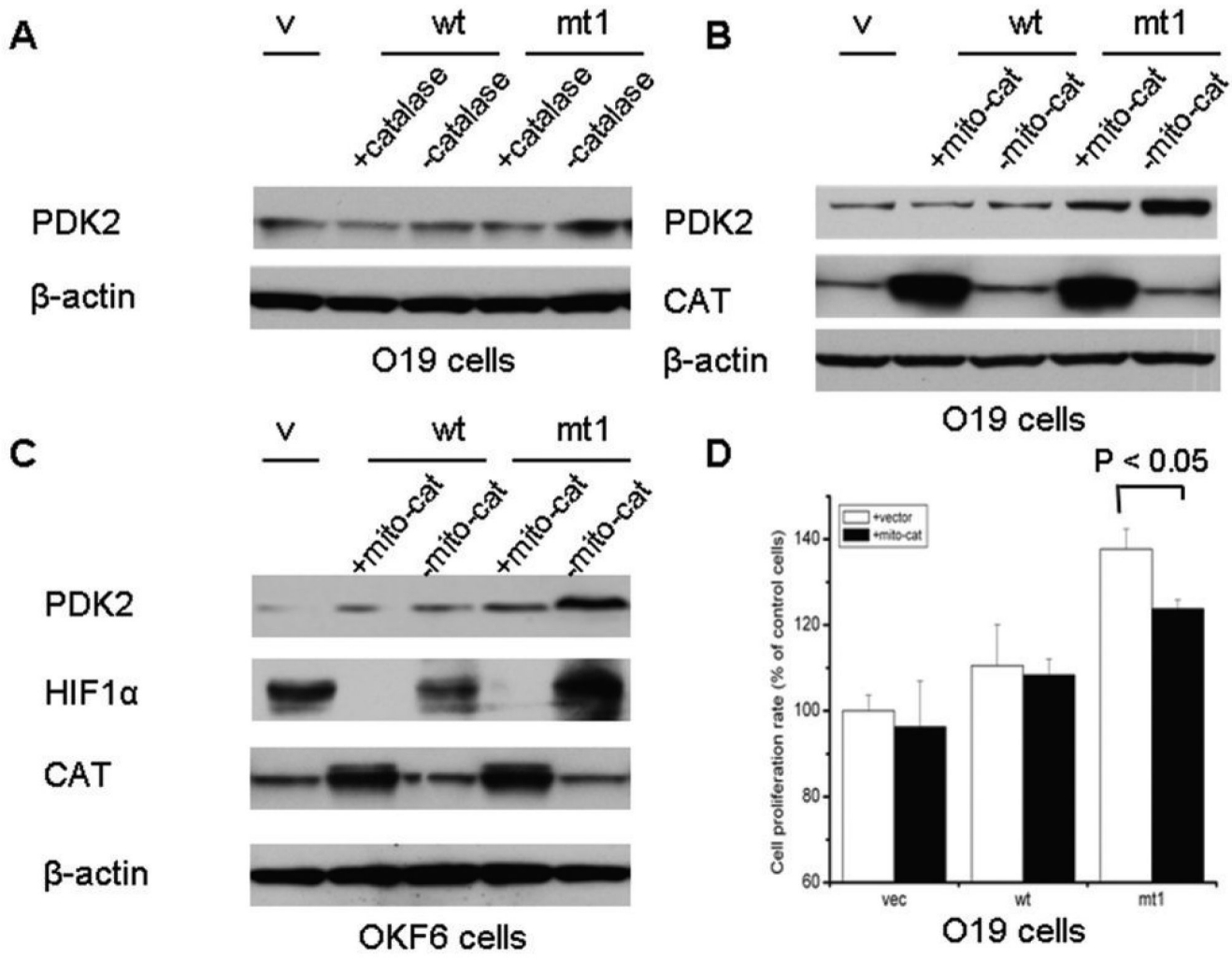

Figure 5.

Inhibition of ROS production in mitochondrial ND2 mutant attenuated PDK2 expression and HIF1α expression. A, PDK2 levels in O19 cells were transiently transfected with ND2 mutant and wild-type construct for 24 h and then subjected to treatment with 500 U/ml catalase for 16 h. The cells were harvested for western blot analysis as described in Materials and methods. +: treated with 500 U/ml catalase for 16 h; -: without catalase treatment. B, PDK2 and HIF1α levels in O19 cells stably transfected with ND2 mutant and wild-type construct, were determined after transiently transfection of plasmid encoding mitocondria-targeted catalase for 48 h. +: transfected with mitochondria-targeted plasmid; -: transfected with control vector alone. C, PDK2 and HIF1α levels in OKF6 cells stably transfected with ND2 mutant and wild-type construct after transient transfection of plasmid encoding mitocondria-targeted catalase for 48 h. +: transfected with mitochondria-targeted plasmid; -: transfected with vector alone. D, the growth of O19 cells with ND2 mutant, was significantly inhibited by transient transfection of plasmid encoding mitocondria-targeted catalase for 48 h ($P<0.05$). Data are representative of results from three independent experiments.

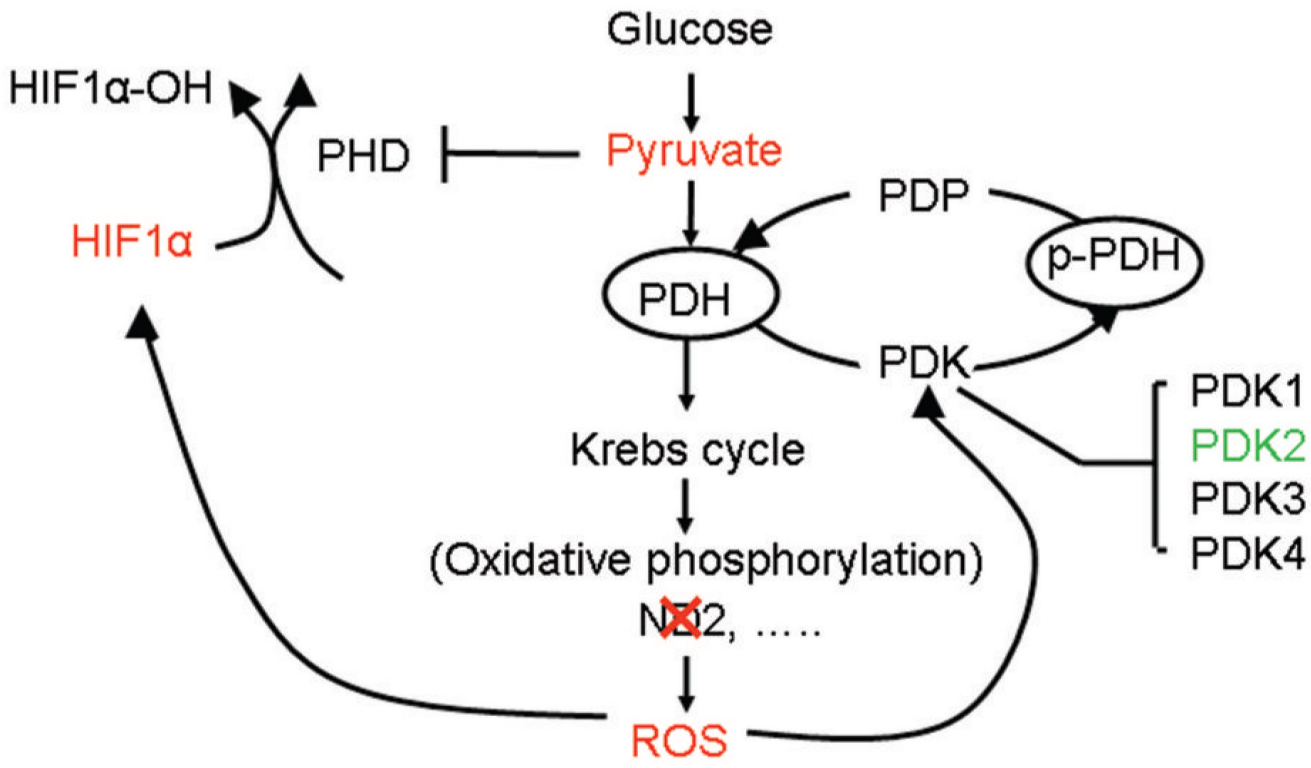

Figure 6.
The mechanisms of mitochondrial ND2 mutation-mediated HIF1α stabilization.